# Time-Resolved Soft X-Ray Imaging of Femtosecond Laser Ablation Processes on Metals

Takuro TOMITA[*1], Masaharu NISHIKINO[*2], Noboru HASEGAWA[*2], Yasuo MINAMI[*3], Ryota TAKEI[*3], Motoyoshi BABA[*3], Takashi EYAMA[*1], Shodai TAKAYOSHI[*1], Takeshi KAIHORI[*2], Toshimasa MORITA[*2], Yusuke HIRANO[*2], Tetsuya KAWACHI[*2], Mitsuru YAMAGIWA[*2] and Tohru SUEMOTO[*3]

[*1] *Faculty of Engineering, The University of Tokushima*
*Tokushima 770-8506, Japan*
*E-mail: tomita@tokushima-u.ac.jp*
[*2] *Quantum Beam Science Directorate, Japan Atomic Energy Agency*
*Umemi-dai, Kizugawa-shi, Kyoto 619-0215, Japan*
[*3] *Institute for Solid State Physics, The University of Tokyo*
*Kashiwanoha, Kashiwa-shi, Chiba 277-8581, Japan*

Femtosecond laser ablation processes on platinum, gold, and tungsten were observed by the single shot pump and probe reflective imaging using a soft x-ray laser probe. To avoid the timing error due to the jitter, we adopted *a posteriori* correction technique by simultaneous measurement of timing between the pump and probe pulses for every single shot, using a soft x-ray streak camera. A clear difference was found in the temporal behavior of the dynamical response of the soft x-ray reflectivity depending on the irradiated laser fluence in these three materials. On the other hand, the narrow dark rings were found in Pt and W, while an additional bright ring was found outside the dark disk in Au. Our result gives the experimental data comparable with various numerical simulations.
DOI: 10.2961/jlmn.2014.02.0011

**Keywords:** femtosecond laser ablation process, time-resolved measurement, soft x-ray laser probe, reflective imaging, platinum, metals

## 1. Introduction

Femtosecond laser ablation, leading to drilling, pattern formation, and surface modification is one kind of the non-repetitive and non-reversible phenomena [1-6]. Although these phenomena are often observed after multiple laser pulse irradiation, it is supposed that the essential material alteration process occurs on single shot base. For example, the pattern formation, such as ripples, is often observed on the several hundreds of nanometer scale, while the fundamental process of the femtosecond laser ablation is suggested to be initiated through the nanometer scaled structure formation, such as nano-bubbles [6]. This means that single-shot observation with the sufficient temporal and spatial resolution is necessary for a better understanding of the femtosecond laser ablation process.

The dynamics of the surface morphology during femtosecond laser ablation has been extensively studied by optical reflectivity and Newton ring-like interference with a time resolution of picosecond by Sokolowski-Tinten *et al.* [7]. Dilatation of the ablation front at a speed of sound velocity was observed. However, the visible light probe cannot give enough spatial resolution to observe the nanostructure formation related the femtosecond laser ablation. In addition, the visible light is shielded by the plasma ejected by the femtosecond laser irradiation. Thus, we suppose that the visible light probe cannot be the most efficient way to understand the femtosecond laser ablation process.

Compared with a visible light, a soft x-ray has extremely short wavelength and the penetration depth of soft x-ray is very shallow. Therefore, the soft x-ray is the most suitable to observe the nanometer scale morphology of the solid surface. Lindenberg *et al*. observed the formation of nano-bubbles in femtosecond laser ablation by using the time-resolved hard x-ray diffuse scattering [8]. Barty *et al*. observed the ablation dynamics of free-standing SiN films by using the soft x-ray beam from the free electron laser [9]. The ablation process and the produced nanoparticles were also studied by inner-shell transitions [10–12]. As for the surface morphological change during the femtosecond laser ablation process, we have reported the observation of the surface expansion in the early stage of femtosecond laser ablation by using the soft x-ray interferometer [13, 14]. The change in optical reflectivity of laser excited material is caused not only by the change of bulk properties due to excited electrons or phase transition (melting), but also by surface deformation and morphology in nanometer scale. Soft x-ray reflectivity depends on the spatial distribution of the atomic density and the roughness of the interface within ten to twenty nanometers from the surface [15]. According to X-Ray Database [16], when the surface roughness increases from 1 nm to 5 nm, the reflectivity reduction exceeds 80 % for our experimental condition. In addition, 20 nm-thick density transition region also causes the reduction of reflectivity of about 80% for the same condition. This high sensitivity of the reflectivity of the soft x-ray to surface morphology brings us rich information about the temporal behavior of the ablation front, which is useful for understanding femtosecond laser ablation dynamics.

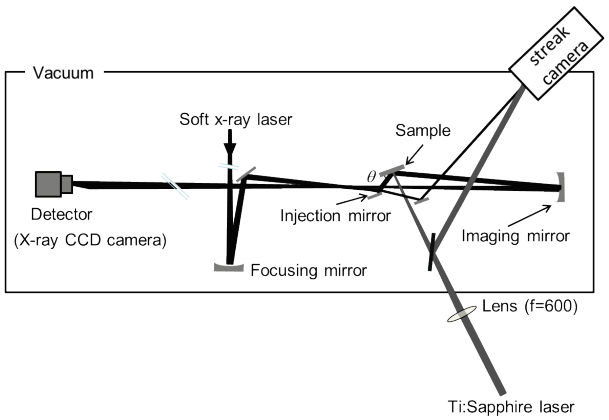


**Fig. 1:** The schematics of the femtosecond laser pump and the soft x-ray reflecting imaging system. The schematics of the timing measurement system between the femtosecond pump beam and the soft x-ray probe beam is also shown in this figure.

In this paper, we demonstrate pump and probe reflective imaging of the platinum (Pt), gold (Au), and tungsten (W) surface during the femtosecond laser ablation by using the laser-driven plasma induced soft x-ray laser (SXRL) as a probe beam. We observed both common and material dependent feature. The obtained data are discussed in comparison with the theoretical calculations.

## 2. Experimental

The laser-driven plasma soft x-ray laser in Japan Atomic Energy Agency (JAEA) was used as the probe beam [17]. The system provides 7 ps soft x-ray pulses, and it delivers soft x-ray photons at 89.2 eV (13.9 nm) with photon number exceeding $10^9$. Owing to this bright laser pulse, it is possible to capture the ultrafast phenomena in single-shot measurement.

Figure 1 shows the schematic setup of the femtosecond laser pump and the soft x-ray probe reflective imaging system. The reflective measurement was carried out in vacuum with a pressure lower than $10^{-3}$ Pa. The soft x-ray probe beam with a wavelength of 13.9 nm from the plasma was focused in front of a sample by the concave mirror. The sample image was transferred onto the detector by the imaging mirror with a magnification factor of 19.1. The injection mirror was placed before the sample in order to adjust the incident grazing angle θ (24.5 degrees) for the sample. The reflectivity is estimated about 30 % for the soft x-ray laser. The detector was a back illuminated charge coupled device (CCD) for soft x-ray (Princeton Instruments, PIXIS-XO: 2048B). The pumping laser used for ablation was a Ti: Sapphire laser system based on chirped pulse amplification (Thales laser, alpha10). The laser emitted 80 fs pulses of linearly polarized light at a central wavelength of 795 nm. The emitted pulses were focused by a lens (f = 600 mm) onto the sample surface at nearly normal incidence. The pumping energy was adjusted by using a combination of a half-wavelength plate and polarizing beam splitter. To evaluate the pulse energy on the sample for each shot, a fraction of the incident pulse was sampled by a photodiode joule meter (OPHIR, PD10-SH-V2).

The *a posteriori* synchronization system between infrared pump and soft x-ray probe beams is also shown in Fig.1. The soft x-ray is divided into two beams at the edge of mirror before the sample in the main beam. Major part of the soft x-ray is reflected by the platinum coated silicon mirror and the minor part is passed through the mirror. The passed light was reflected by another mirror placed behind the first mirror and directed to the soft x-ray streak camera. The major part of the beam was irradiated onto the surface of

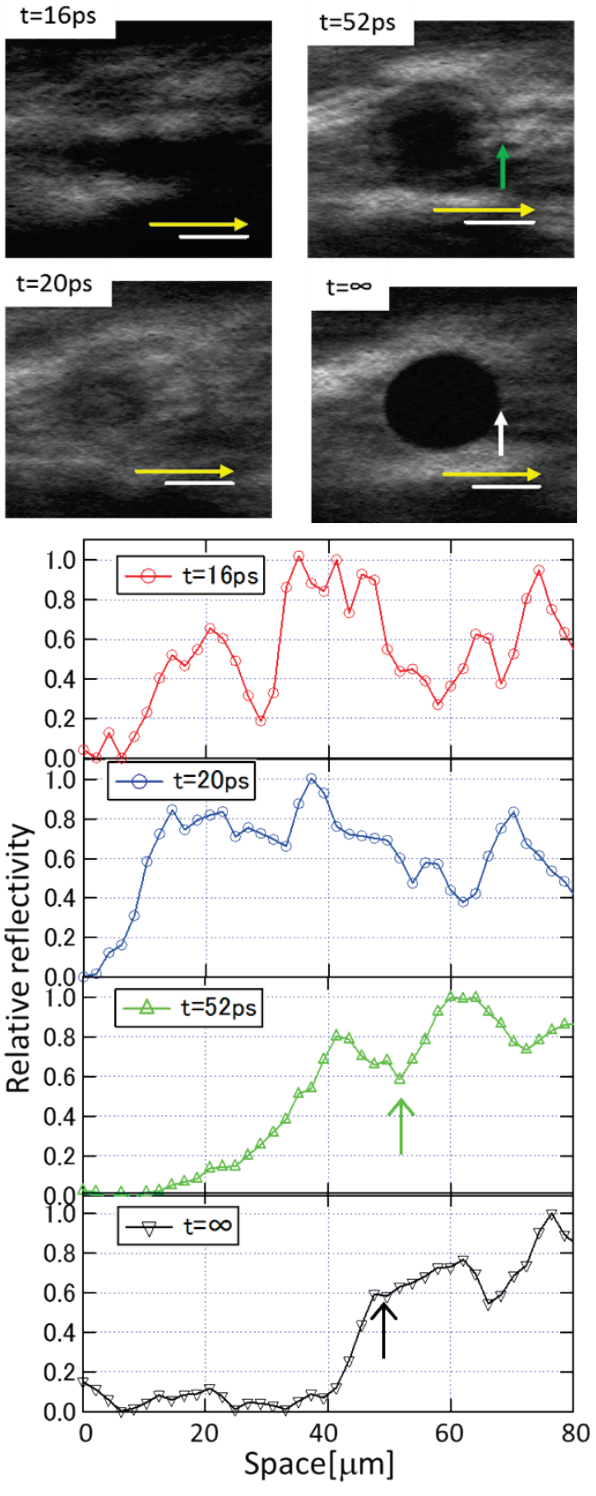


**Fig. 2:** The top photographs show the soft x-ray reflectivity images on platinum at various delay times. The scale bar corresponds to 50 μm. The reflectivity as a function of the radial position (fluence dependence) is plotted in the bottom graph. The yellow arrow in the image shows the direction and length of the cross-sectional plots. Note that this arrow shifted vertical direction only for convenient display.

the sample and directed to the CCD camera. The pump beam is also divided into two beams by a beam splitter placed before the vacuum chamber. The time origin was determined for every single shot by simultaneous observation of the signals of soft x-ray and multi-photon photoemission signal of the pump pulse, using an x-ray streak camera (Hamamatsu Photonics, C4575-01). This timing measurement technique was introduced in order to eliminate the timing error due to the jitter and the accuracy of time was significantly improved (< 2 ps) compared to our previous result (~10ps) [18].

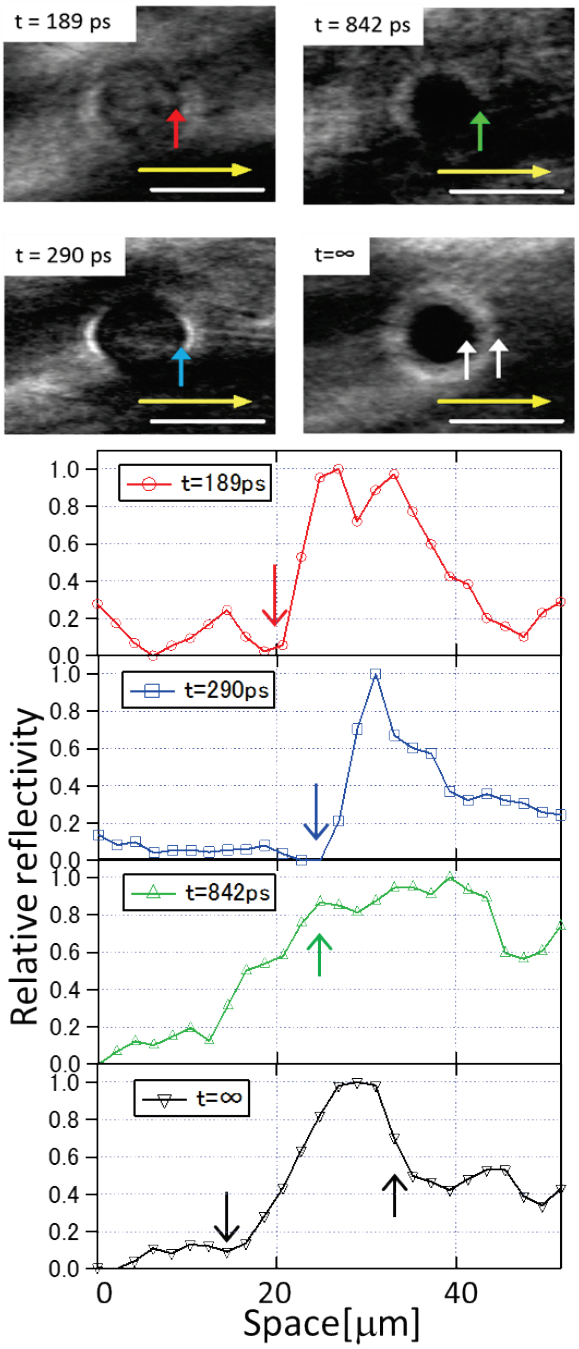


**Fig. 3:** The top graph shows the soft x-ray reflectivity images on gold at various delay times. The scale bar corresponds to 50 μm. The reflectivity as a function of the radial position (fluence dependence) is plotted in the bottom graph. The yellow arrow in the image shows the direction and length of the cross-sectional plots. Note that this arrow shifted vertical direction only for convenient display.

The pump beam had a Gaussian shaped intensity profile and the focal spot sizes (1/e) on the sample surface were measured to be about 54 μm for Pt and Au and about 100 μm for W. The typical pump energy, peak fluence, and excitation intensity on the sample surface were 170 μJ, 4.1 J/cm$^2$, and $1\times10^{14}$ W/cm$^2$, respectively. The Gaussian shaped intensity profiles enables us to discuss the local fluence dependence by discuss the radial position dependence of the ablation phenomena.

The samples were Pt, Au, and W thin films with 300 nm, 100 nm, and 113 nm thicknesses evaporated on fused silica substrates, respectively. We chose these metals for the sample because of their high reflectivity to the soft x-ray and the various melting points. The initial surface roughness was measured by atomic force microscope (AFM) and the root mean square (RMS) deviation was found less than 1.0 nm.

## 3. Results and Discussion

Figure 2 shows the soft x-ray reflective images of Pt surface at different delay times after the irradiation of the pump pulse. The peak fluence was 1.1 J/cm$^2$. The scale-bar corresponds to 50 μm for all images in Fig. 2, and the contrast was optimized for each image. On Pt, the dark disk was observed after 20 ps, and a dark ring outside the dark disk was observed at 52 ps. The dark disk expands toward the outside and stops its growing when the radius of the dark disk coincides with that of the dark ring.

The intensity non-uniformity observed outside the disk-shaped dark area stems mainly from the spatial non-uniformity of the soft x-ray. The cross-section of the relative reflectivity normalized to the intensities where the brightest reflectivity was observed is shown in the bottom of Fig. 2.

On the contrary, the reflectivity change on Au, shown in Fig. 3, is much slower than that on Pt. A dark disk is observed at 189 ps and persists to spread out up to about 1 ns. The peak fluence was 1.1 J/cm$^2$. The scale-bar corresponds to 50 μm for all images in Fig. 3, and the contrast was optimized for each image. The cross-section of the relative reflectivity normalized to the intensities where the brightest reflectivity was observed is shown in the bottom of Fig. 3. Interestingly, in contrast to the other metals, the bright ring structure was observed outside the dark disk at t=189, 290, 842, ∞ ps. In addition, the size of the dark disk seemed to shrink at t=842 ps. The reason why this shrinkage is not clear yet, it is possible that the transient melt is occurred at the time.

On W, the observed reflectivity change, shown in Fig.4, is similar to that on Pt. The peak fluence was 0.6 J/cm$^2$. The scale-bar corresponds to 50 μm for all images in Fig. 4, and the contrast was optimized for each image. We have plotted the cross-sections of the soft x-ray reflectivity on W in Fig. 4. The cross-section of the relative reflectivity normalized to the intensities where the brightest reflectivity was observed is shown in the bottom of Fig. 4. It is worth noting that the width of the dark ring at t = 30 ps, indicated by red arrow, is very narrow compared to that on Pt.

The difference in the temporal behavior of the reflectivity indicates that the observed phenomena are strongly fluence dependent. Thus, in the following, we will discuss the

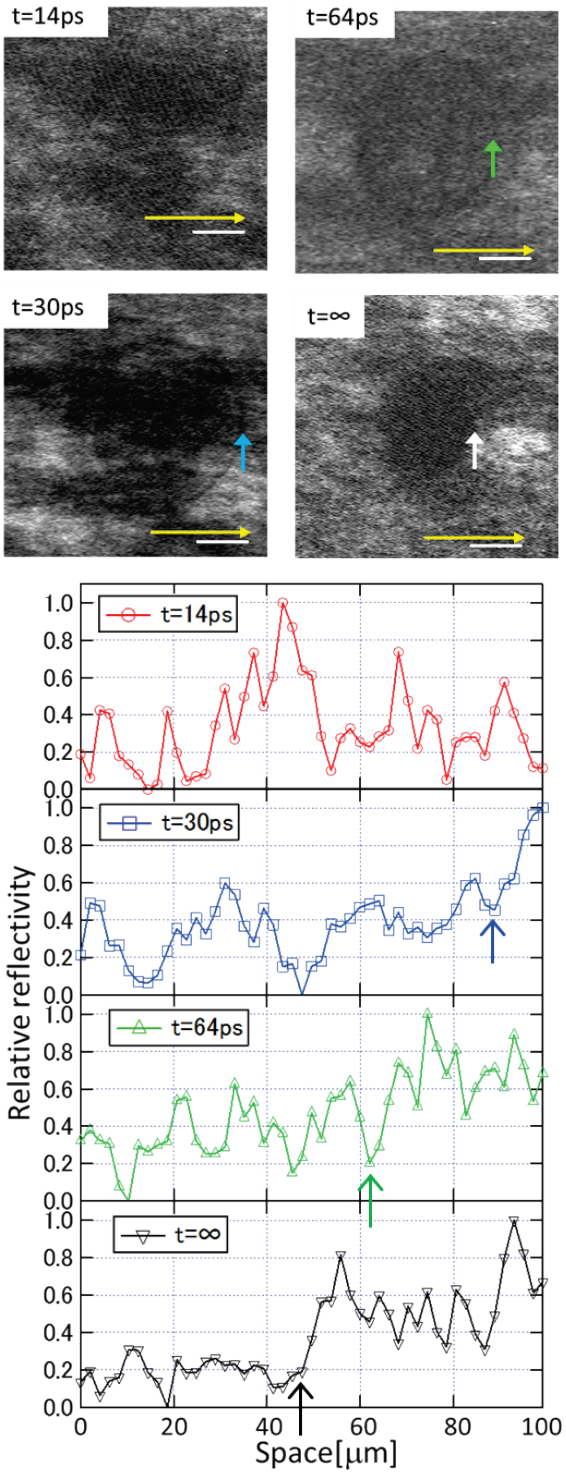


**Fig. 4:** The top graph shows the soft x-ray reflectivity images on tungsten at various delay times. The scale bar corresponds to 50 μm. The reflectivity as a function of the radial position (fluence dependence) is plotted in the bottom graph. The yellow in the image arrow shows the direction and length of the cross-sectional plots. Note that this arrow shifted vertical direction only for convenient display.

origin of the reflectivity drop at t =+∞. The origin of the reflectivity drop is ascribed to the random nano-structure at the bottom of the crater as discussed below. It is reported that the femtosecond laser induces nanometer-scaled roughness on metal surface [19, 20]. We examined the surface morphologies inside the crater at t =+∞ by AFM. The typical values of the surface roughness were several tens of nanometers, and the correlation lengths along the surface plane of the roughness were smaller than 1 μm. For evaluating the x-ray reflectivity of a rough surface, the Nevot-Croce factor is known to be a good approximation when the roughness spectrum has a high spatial frequency (>1μm$^{-1}$) [21]. According to this formulation, we estimated the reflectivity to be negligibly small (less than $10^{-40}$). Thus, we ascribed the observed reflectivity drop at t =+∞ to the surface roughness.

Next, we will discuss the origin of the transient soft x-ray reflectivity change. As the origin of the change of the intensity of the reflected soft x-ray, there are several possibilities, that is, ejected plasma, nanoparticles and change of the surface morphology of the sample. Since plasma might be ejected from the surface at a high pumping fluence exceeding $10^{13}$ W/cm$^2$, we evaluated the time-space behavior of the electron density by using the hydrodynamic code HYADES [19], assuming rectangular pulse with a width of 100-200 fs and power density of $10^{13}$ W/cm$^2$ for pumping. According to this calculation, a layer several tens of nanometers from the top starts to expand around 10 ps, and the plasma expands to a height of 60 nm at 40 ps. However, the density is far smaller than the reflection limit of the 13.9 nm light (= 24.5×10 cm$^{-3}$), and reflectance will be negligible.

The generation of nanoparticles of the target material is also the possible origin of the observed reflectivity drop. However, the density of nanoparticles is not so high as to disturb the transmission of the soft x-ray [22–24]. Thus, we suppose that the observed reflectivity drop is caused by the surface morphologies of the target materials.

According to the above discussion, we concluded that the dark disks at the center of the irradiated spot can be attributed to the density gradient of the materials associated to the femtosecond laser ablation. In addition, the dark rings at the edge of the ablation crater arise from the surface roughness of the irradiated materials in the ablation process. Furthermore, the bright spots at the edge of the ablation crater in the horizontal direction, which may be affected by the reflection geometry of the probe beam, (Fig. 3, t=290 ps) is probably ascribed to reduced roughness after re-solidification of the Au surface.

For understanding the origin of the transient morphological change, numerical simulation of the ablation process is helpful. One is the calculation assuming Lennard-Jones potential. From this calculation, the spallation, homogeneous nucleation, fragmentation, and vaporization processes are predicted as the ablation process with increasing laser fluence [25, 26]. The reflectivity of the soft x-ray strongly depends on the surface roughness, the reduction of material density, and the density gradient near the surface of the material. Our observation showed that there are two distinct areas inside the crater; the reflectivity in the central area shows rapid decrease and the outer area show delayed decrease in Pt, Au and W. In addition, a narrow area near the crater edge shows a sharp reflectivity decrease at the very early stage. These behaviors may correspond to these predicted different ablation schemes

Another possible explanation of our experimental results can be given by the model proposed by Zhigilei *et al.* [27, 28], where metal ablation is treated assuming electron and

lattice temperatures independently (two-temperature model). In their simulation, separation of a liquid layer (spallation) from the substrate is observed above ablation threshold.

As we have reported, the fluence dependence of the dynamical behavior showed threshold behavior in Pt [18]. We have tentatively compared our results with the theoretical model by Lewis *et al.* or Zhigilei *et al.* [25-28]. However, the model reported by Lewis [25, 26] was based on the Lennard-Jones potential, which assumes insulating sample. On the other hand, the models by Zhigilei *et al.* calculated the femtosecond ablation process by assuming metal samples. Although the basic behavior could be understood in terms of these calculations, more sophisticated theoretical models are required, for understanding the material dependent behavior. For example, the ablation rate is much slower in Au than that in Pt and W. The shrinkage of the dark disk of soft x-ray reflectivity cannot be explained, too. In addition, the slow ablation process observed on Au in our experiment may be related to the unique physical properties in gold [29], and the effects of hydrodynamic expansion may be related to the observed material dependence of the ablation phenomena [30].

According to the above discussion, we can find the advantages and disadvantages on each models. Therefore, more detailed numerical simulation for specified material and the calculation of the expected optical properties of the interface in the soft x-ray region are needed for the precise comparison between the theoretical model and the experimental results.

## 4. Conclusion

Ti:Sapphire laser pump and soft x-ray laser imaging of the reflectivity was carried out for the observation of femtosecond laser ablation dynamics on Pt, Au, and W films. By using the Gaussian profiled beam, the fluence dependence of laser-induced phase transition process was deduced. Regardless the continuous intensity profile of the pump beam, the dynamical behavior of soft x-ray reflectivity showed discontinuous irradiation fluence dependence. The further comparison between experimental results and the numerical calculation is needed for the better understanding of the femtosecond laser ablation process.

**Acknowledgment**

The results were achieved under the Facilities Utilization system of Japan Atomic Energy Agency. This work was partially supported by JSPS KAKENHI Grant-in-Aid for Scientific Research on Innovative Areas Grant Number 24110712, and Grant-in-Aid for Scientific Research (B) Grant Number 25286086.

**References**

[1] E. G. Gamaly, S. Juodkazis, K. Nishimura, H. Misawa, B. Luther-Davies, L. Hallo, P. Nicolai, and V. T. Tikhonchuk: Phys. Rev. B, 73, (2006) 214101.

[2] F. Korte, J. Koch, and B. N. Chichkov: Appl. Phys. A, 79, (2004) 879.

[3] A. Pereira, A. Cros, P. Delaporte, S. Georgiou, A. Manousaki, W. Marine, and M. Sentis: Appl. Phys. A, 79, (2004) 1433.

[4] T -H. Her, R. J. Finlay, C. Wu, S. Deliwala, and E. Mazur: Appl. Phys. Lett., 73, (1998) 1673.

[5] F. Korte, J. Serbin, J. Koch, A. Egbert, C. Fallnich, A. Ostendorf, and B. B. Chichkov: Appl. Phys. A, 77, (2003) 229.

[6] D. von der Linde, K. Sokolowski-Tinten, and J. Bialkowski: Appl. Surf. Sci., 109-110, (1997) 1.

[7] K. Sokolowski-Tinten, J. Bialkowski, A. Cavalleri, D. von der Linde, A. Oparin, J. Meyer-ter-Vehn, and S. I. Anisimov: Phys. Rev. Lett., 81, (1998) 224.

[8] A. M. Lindenberg, S. Engemann, K. J. Gaffney, K. Sokolowski-Tinten, J. Larsson, P. B. Hillyard, D. A. Reis, D. M. Fritz, J. Arthur, R. A. Akre, M. J. George, A. Deb, P. H. Bucksbaum, J. Hajdu, D. A. Meyer, M. Nicoul, C. Blome, Th. Tschentscher, A. L. Cavalieri, R.W. Falcone, S. H. Lee, R. Pahl, J. Rudati, P. H. Fuoss, A. J. Nelson, P. Krejcik, D. P. Siddons, P. Lorazo, and J. B. Hastings: Phys. Rev. Lett., 100, (2008) 135502.

[9] A. Barty, S. Boutet, M. J. Bogan, S. Hau-Riege, S. Marchesini, K. Sokolowsli-Tinten, N. Stojanovic, R. Tobey, H. Ehrke, A. Cavalleri, S. D¨usterer, M. Frank, S. Bajt, B. W. Woods, M. M. Seibert, J. Hajdu, R. Treusch, and H. N. Chapman: Nature Photonics, 2, (2008) 415.

[10] T. E. Glover, G. D. Ackerman, A. Belkacem, P. A. Heimann, Z. Hussain, R. W. Lee, H. A. Padmore, C. Ray, R. W. Schoenlein, W. F. Steele, and D. A. Young: Phys. Rev. Lett., 90, (2003) 236102.

[11] K. Oguri, Y. Okano, T. Nishikawa, and H. Nakano: Phys. Rev. B, 79, (2009) 144106.

[12] K. Oguri, Y. Okano, T. Nishikawa, and H. Nakano: Phys. Rev. Lett., 99, (2007) 165003.

[13] T. Suemoto, K. Terakawa, Y. Ochi, T. Tomita, M. Yamamoto, N. Hasegawa, M. Deki, Y. Minami, and T. Kawachi: Opt. Express, 18, (2010) 14114.

[14] Y. Ochi, K. Terakawa, N. Hasegawa, M. Yamamoto, T. Tomita, T. Kawachi, Y. Minami, M. Nishikino, T. Imazono, M. Ishino, and T. Suemoto: Jpn. J. Appl. Phys., 51, (2012) 016601.

[15] M. Yanagihara, T. Sasaki, M. Furudate, and M. Yamamoto: Opt. Rev., 3, (1996) 65.

[16] http://henke.lbl.gov/optical constants/

[17] Y. Ochi, T. Kawachi, N. Hasegawa, M. Nishikino, T. Ohba, M. Tanaka, M. Kishimoto, T. Kaihori, K. Nagahima, and A. Sugiyama: Jpn. J. Appl. Phys., 48, (2009) 120212.

[18] T. Tomita, M. Yamamoto, N. Hasegawa, K. Terakawa, Y. Minami, M. Nishikino, M. Ishino, T. Kaihori, Y. Ochi, T. Kawachi, M. Yamagiwa and T. Suemoto: Opt. Express, 20, (2012) 29329.

[19] A. Y. Vorobyev, and C. Guo: Opt. Express, 14, (2006) 2164.

[20] A. Y. Vorobyev, V. S. Makin, and C. Guo: J. Appl. Phys., 101, (2007) 034903.

[21] K. Stoev, and K. Sakurai: Rigaku J., 14, (1997) 22.

[22] O. Albert, S. Roger, Y. Glinec, J. C. Loulergue, J. Etchepare, C. Boulmer-Leborgne, J. Perrière, and E. Millon: Appl. Phys. A, 76, (2003) 319.

[23] S. Amoruso, R. Bruzzese, N. Spinelli, R. Velotta, M. Vitiello, and X. Wang: Europhys. Lett., 67, (2004) 404.

[24] S. Eliezer, N. Eliaz, E. Grossman, D. Fisher, I. Gouzman, Z. Henis, S. Pecker, Y. Horovitz, M. Fraenkel, S. Maman, and Y. Lereah: Phys. Rev. B, 69, (2004) 144119.

[25] D. Perez, and L. J. Lewis: Phys. Rev. B, 67, (2003) 184102.
[26] P. Lorazo, L. J. Lewis, and M. Meunier: Phys. Rev. B, 73, (2006) 134108.
[27] B. J. Garrison, T. E. Itina, and L. V. Zhigilei: Phys. Rev. E, 68, (2003) 041501.
[28] L. V. Zhigilei, Z. Lin, and D. S. Ivanov: J. Phys. Chem. C 113, (2009) 11892.
[29] S. Mazevet, J. Clérouin, V. Recoules, P. M. Anglade, and G. Zerah, Phys. Rev. Lett. 95, (2005) 085002.
[30] J. P. Colombier, P. Combis, E. Audouard, and R. Stoian: New J. Phys. 14, (2012) 013039.

(Received: July 19, 2013, Accepted: April 15, 2014)